Article

Differential Redox Regulation of Ca^{2+} Signaling and Viability in Normal and Malignant Prostate Cells

Christian Holzmann,[1] Tatiana Kilch,[1,2] Sven Kappel,[1] Kathrin Dörr,[1] Volker Jung,[3] Michael Stöckle,[3] Ivan Bogeski,[1] and Christine Peinelt[1,2,*]

[1]Biophysics, Center for Integrated Physiology and Molecular Medicine, School of Medicine, [2]Center of Human and Molecular Biology, and [3]Clinics of Urology and Pediatric Urology, Saarland University, Homburg, Germany

ABSTRACT In prostate cancer, reactive oxygen species (ROS) are elevated and Ca^{2+} signaling is impaired. Thus, several novel therapeutic strategies have been developed to target altered ROS and Ca^{2+} signaling pathways in prostate cancer. Here, we investigate alterations of intracellular Ca^{2+} and inhibition of cell viability caused by ROS in primary human prostate epithelial cells (hPECs) from healthy tissue and prostate cancer cell lines (LNCaP, DU145, and PC3). In hPECs, LNCaP and DU145 H_2O_2 induces an initial Ca^{2+} increase, which in prostate cancer cells is blocked at high concentrations of H_2O_2. Upon depletion of intracellular Ca^{2+} stores, store-operated Ca^{2+} entry (SOCE) is activated. SOCE channels can be formed by hexameric Orai1 channels; however, Orai1 can form heteromultimers with its homolog, Orai3. Since the redox sensor of Orai1 (Cys-195) is absent in Orai3, the Orai1/Orai3 ratio in T cells determines the redox sensitivity of SOCE and cell viability. In prostate cancer cells, SOCE is blocked at lower concentrations of H_2O_2 compared with hPECs. An analysis of data from hPECs, LNCaP, DU145, and PC3, as well as previously published data from naive and effector T_H cells, demonstrates a strong correlation between the Orai1/Orai3 ratio and the SOCE redox sensitivity and cell viability. Therefore, our data support the concept that store-operated Ca^{2+} channels in hPECs and prostate cancer cells are heteromeric Orai1/Orai3 channels with an increased Orai1/Orai3 ratio in cells derived from prostate cancer tumors. In addition, ROS-induced alterations in Ca^{2+} signaling in prostate cancer cells may contribute to the higher sensitivity of these cells to ROS.

INTRODUCTION

Numerous studies have demonstrated a contribution of reactive oxygen species (ROS) to the development of cancer hallmarks. In prostate cancer, ROS levels are elevated and contribute to altered DNA and protein structures, enhanced epithelial cell proliferation, and neoplasia (1–5). Remarkably, even though ROS production in cancer cells is elevated, cancer cells (including prostate cancer cells) are more sensitive to oxidative stress than nonmalignant cells—a phenomenon that is utilized in the development of novel anticancer drugs (6,7). ROS-inducing substances and ROS scavengers have been investigated as therapeutics; however, the outcome and benefit of such strategies remain largely unclear (8). Therefore, a better understanding of the underlying mechanisms and key players in redox-regulated signaling pathways is required for future therapeutic approaches.

There are multiple links between ROS and the universal second messenger Ca^{2+} (9–11). In prostate cancer cells, ROS-induced signaling is well known to include elevated Ca^{2+}. In PC3 prostate cancer cells, ROS was shown to induce an increase of intracellular Ca^{2+} levels, which is necessary for ROS-induced apoptosis (12). In DU145 cells, ROS-activated cell apoptosis depends on elevated Ca^{2+} signaling for a full response (13). Several Ca^{2+} transporters, including transient receptor potential (TRP) channels and inositol 1,4,5-trisphosphate receptors (IP_3R), which are activated and/or regulated by ROS, contribute to ROS-induced Ca^{2+} signaling (14–17). The cell-type-specific subset of Ca^{2+} transporters and the distinct and spatially complex regulation of ROS by ROS-producing and -scavenging enzymes ensure precise ROS-induced Ca^{2+} signaling patterns (14,18).

The main Ca^{2+} entry mechanism in nonexcitable cells is known as store-operated Ca^{2+} entry (SOCE). Upon Ca^{2+} release from internal Ca^{2+} stores, endoplasmic reticulum Ca^{2+} sensor proteins (e.g., stromal interaction molecule 1 (STIM1)) cluster and activate Orai1 Ca^{2+} channels that are located in the plasma membrane (19). The SOCE underlying current is referred to as Ca^{2+} release activated Ca^{2+} current (I_{CRAC}). Store-operated Orai1 channels have been described as either tetramers (20–25) or hexamers (26–29) in the past. Besides Orai1, Orai2 and Orai3 are ubiquitously expressed and form heteromers with Orai1 (30–33). Compared with homomeric Orai1 channels, heteromeric store-operated Orai1/Orai3 channels differ in certain properties, such as the Ca^{2+} current amplitude, ion selectivity, pharmacological profile, and ROS sensitivity (33–36). A very recent report demonstrated that one Orai3 subunit within a heteromeric channel complex is sufficient to completely abrogate the ROS sensitivity of I_{CRAC} (37).

Submitted March 11, 2015, and accepted for publication August 6, 2015.

*Correspondence: bpcpei@uks.eu

Editor: Michael Pusch.

0006-3495/15/10/1410/10

http://dx.doi.org/10.1016/j.bpj.2015.08.006

The ROS sensitivity of Orai1 has been attributed to the oxidation of one cysteine (Cys-195). Since Cys-195 is absent in Orai3, the Orai1/Orai3 expression ratio impacts the ROS-mediated block of SOCE and cellular viability upon ROS-mediated stress. In effector T cells, Orai3 is upregulated, as reflected by a decreased mRNA ratio (Orai1/Orai3 ratio ~70 in naive T_H cells and ~25 in effector T_H cells) (35). Subsequently, the IC_{50} for the immediate H_2O_2-induced block of SOCE is shifted from 7 μM for naive T_H cells to 51 μM for effector T_H cells. As a physiological consequence, the lowered Orai1/Orai3 ratio increases the cellular viability upon oxidative stress (IC_{50} = 39 μM H_2O_2 in naive T_H cells, and IC_{50} = 199 μM H_2O_2 in effector T_H cells) (35). These relatively high levels of H_2O_2 seem to be physiologically relevant. Based on our recent findings (38,39), and taking into account previous concepts regarding the existence of ROS microdomains (40–42), it seems very likely that in inflamed tissues the levels of H_2O_2 might well exceed 200–300 μM.

Recently, we reported an outstandingly low Orai1/Orai3 mRNA ratio (~4) in primary human prostate epithelial cells (hPECs) from healthy tissue and a downregulation of Orai3 in prostate cancer cell lines (Orai1/Orai3 ratio ~26 in lymph node carcinoma of the prostate (LNCaP) and ~17 in DU145) (34).

Here, we sought to determine whether ROS-induced Ca^{2+} signaling and SOCE in cells under oxidative stress are altered in prostate cancer. In addition, we investigated whether the low Orai1/Orai3 ratio in hPECs is associated with a low redox sensitivity of SOCE, and whether this sensitivity might be increased in prostate cancer cells.

MATERIALS AND METHODS

Cell culture

This study was approved by the local ethics review board (approval No. 168/05, Ärztekammer des Saarlandes) and performed in accordance with the Declaration of Helsinki. Informed consent was obtained from all patients. Prostate tissue was obtained from prostectomy specimens, and hPECs obtained from healthy tissue were isolated and cultured according to Gmyrek et al. (43) with slight modifications (34). The prostate cancer lines LNCaP, DU145, and PC3 were purchased from the American Type Cell Culture Collection (ATCC, Rockville, MD). Cell lines were cultured with RPMI Medium 1640 (Life Technologies) supplemented with 10% fetal calf serum and 1% penicillin/streptomycin (Life Technologies).

Small interfering RNA transfection

Small interfering RNA (siRNA) transfections were performed as described previously (34). We performed the siRNA transfections with 0.12 nmol of siRNA using the Nucleofector II Transfection Kit R for hPECs and LNCaP, the Nucleofactor IV Kit SE for DU145, and the Kit SF for PC3 (all from Lonza) according to the manufacturer's instructions. All siRNAs were obtained from Qiagen or Microsynth and were partially modified according to Mantei et al. (44). The Orai1 siRNAs were Hs_TMEM142A_1, #SI03196207 (sense: 5′OMeC-OMeG-GCCUGAUCUUUAUCGd (UCU) OMeU-OMeT-OMeT3′; antisense: 3′OMeG-OMeC-CGGACUAGAAAUA GCAGAd (A)5′) and Hs_TMEM142A_2, #SI04215316 (sense: 5′OMeC-OMeA-ACAUCGAGGCGGUGA) d(GCA) OMeA-OMeT-OMeT3′; antisense: 3′OMeG-OMeT-UGUAGCUCCGCCACUCGUd (U)5′). The Orai3 siRNAs were Hs_TMEM142C_2, #SI04174191 (sense: 5′OMeC-OMeA-CCAGUGGCUACCUCCd(CUU) OMeA-OMeTOMeT3′; antisense: 3′OMeG-OMeT-GGUCACCGAUGGAGGGAAd(U)5′) and Hs_TMEM 142C_5, #SI04348876 (sense: 5′OMeT-OMeC-CUUAGCCCUUGAAAU) d(ACA) OMeA-OMeT-OMeT3′; antisense: 3′OMeA-OMeG-GAAUCGG GAACUUUAUGUd(U)5′). The STIM1 siRNAs were Hs_STIM1_5, #SI03235442 (sense: 5′OMeU-OMeGAGGUGGAGGUGCAAUd (AUU) dOMeA-dOMeT-dOMeT3′; antisense: 3′OMeA-OMeC-UCCACCUCCAC GUUAUAAd (U)5′) and Hs_STIM1_6, #SI04165175 (sense: 5′OMeC-OMeU-GGUGGUGUCUAUCGUd (UAU) OMeU-OMeT-OMeT3′; antisense: 3′OMeG-OMeA-CCACCACAGAUAGCAAUAd (A)5′).

Control cells were transfected with nonsilencing RNA MS_control_mod (sense: 5′OmeA-OMeA-AGGUAGUGUAAUCGCd(CUU) OMeG-OmeT-OMeT3′; antisense: 3′OmeT-OmeT-UCCAUCACAUUAGCGGAAdC 5′).

Quantitative real-time PCR

Quantitative real-time PCR (qRT-PCR) was performed as previously described (34). Total RNA from LNCaP, DU145, PC3, and hPECs was isolated with TRIzol Reagent (Life Technologies). For reverse transcription, 0.8 μg of isolated total RNA was used.

The QuantiTect SYBR Green Kit (Qiagen) was used with 0.5 μL of complementary DNA and 300 nM of primer. The PCR conditions were as follows: 15 min at 95°C; 45 cycles, 30 s at 95°C; 45 s at 58°C; and 30 s at 72°C, and finally a cycle (60 s, 95°C; 30 s 55°C; 30 s 95°C) to determine specificity by a dissociation curve using the MX3000 cycler (Stratagene). Expression of target genes were normalized to the expression of the reference genes RNA polymerase II (RNAPol, NM_000937) and/or TATA box binding protein (TBP, NM_003194). The primer sequences were as follows: Orai1, 5′atgagcctcaacgagcact3′ (forward) and 5′gtgggtagt cgtggtcag3′ (reverse); Orai3, 5′gtaccgggagttcgtgca3′ (forward) and 5′ggta ctcgtggtcactct3′ (reverse); STIM1, 5′ cagagtctgcatgaccttca 3′ (forward) and 5′ gcttcctgcttagcaaggtt 3′ (reverse); TBP, 5′ cggagagttctgggattgt 3′ (forward) and 5′ ggttcgtggctctcttatc 3′ (reverse); and RNAPol, 5′ ggagattgagtc caagttca 3′ (forward) and 5′ gcagacacaccagcatagt 3′ (reverse).

Ca^{2+} imaging experiments

Cells were loaded with the ratiometric dye Fura-2AM (hPECs: 1 μM/37°C/20 min; LNCaP and DU145: 2 μM/37°C/15 min; and PC3: 4 μM/room temperature/45 min). Excitation light alternated between 340 nm and 380 nm, and emitted light was detected every 5 s at an emission wavelength of 440 nm. Data were analyzed with TILLVision software (TILL Photonics) and IGOR Pro (WaveMetrics), and intracellular Ca^{2+} concentrations were determined as described previously (45,46).

The bath solution contained (in mM) 155 NaCl, 4.5 KCl, 2 $MgCl_2$, 10 glucose, and 5 HEPES (pH 7.4 with NaOH). H_2O_2, $CaCl_2$, and 1 μM thapsigargin (Tg) were added as indicated.

Electrophysiology

Cells (LNCaP and DU145) were patched in a whole-cell configuration as described previously (47,48). The pipette resistance was 2–4 MΩ. Every 2 s, 50 ms spanning ramps from −150 to +100 mV were delivered from a holding potential of 0 mV by a HEKA EPC-10 patch-clamp amplifier and the data were filtered (2.9 Hz), recorded, and analyzed with the use of Patchmaster and Fitmaster software (HEKA). The liquid junction potential was corrected for 10 mV. For analysis, currents were extracted at −80 mV, normalized to the cell capacity, averaged, and plotted versus

time. Current was plotted versus ramp voltage (I/V), and current density (CD) was plotted versus H_2O_2 dose and fitted with a Hill function. The pipette solution contained (in mM) 120 Cs-glutamate, 10 BAPTA, 10 HEPES, 3 $MgCl_2$, and 0.05 IP_3. The bath solution contained (in mM) 95 NaCl, 2.8 KCl, 20 $CaCl_2$, 2 $MgCl_2$, 10 HEPES, 10 TEA-Cl, 10 CsCl, and 10 glucose. The pH was adjusted with NaOH to 7.2 and the osmolarity was 300 mosmol/L. H_2O_2 was added as indicated and cells were incubated for 10–30 min before patch-clamp experiments were conducted.

Cell viability

hPEC, LNCaP, DU145, and PC3 cells were seeded to ~80% density in 96-well cell culture plates (BD) and incubated at 37°C, 5% CO_2, and 95% humidity. Living cells were detected by means of a CellTiter-Blue assay (Promega). The sample size was $n = 12$ for LNCaP, $n = 9$ for DU145, $n = 3$ for PC3, and $n = 22$ from three donors of hPECs.

Data analysis

Data were analyzed using TILLVision, Fitmaster, Igor Pro, and Microsoft Excel. Data are given as the mean ± SE. (For the data plotted in Fig. 7, Pearson's coefficient was calculated and is indicated as the R value.)

RESULTS

hPECs and prostate cancer cells differ in Ca^{2+} signaling upon incubation with H_2O_2

We first tested the effect of H_2O_2 on Ca^{2+} signaling in a Fura-2-based Ca^{2+} imaging assay in hPECs and the cancer cell lines LNCaP and DU145. For the later analysis of previously published data and data from this study, we exactly followed the procedure published earlier (35). Cells were incubated with different concentrations of H_2O_2, and SOCE was activated with the SERCA inhibitor Tg.

Average Ca^{2+} responses with different H_2O_2 concentrations are shown in Fig. 1, *A–C*. Incubation of hPECs, LNCaP, and DU145 with H_2O_2 first induced an initial increase of intracellular Ca^{2+}. Upon application of Tg, intracellular Ca^{2+} increased (Fig. 1, *A–C*). To test the contribution of STIM/Orai-mediated signaling, we next analyzed the dependence of the initial Ca^{2+} increase and the Tg-induced intracellular Ca^{2+} increase on the main molecular components of SOCE, STIM1 and Orai1.

Dependence of the initial Ca^{2+} increase and the Tg-induced intracellular Ca^{2+} increase on STIM1 and Orai1

To investigate whether the initial Ca^{2+} increase and the Tg-induced intracellular Ca^{2+} increase depend on SOCE, we performed an siRNA-based knockdown of the main molecular components of SOCE, STIM1 and Orai1.

In LNCaP cells, knockdown of STIM1 and Orai1 efficiently reduced the mRNA levels of STIM1 and Orai1 (Fig. 2 *A*). We then performed the same Fura-2-based imaging experiment shown in Fig. 1 in cells that were transfected with control RNA or siRNA targeting STIM1 and Orai1 (Fig. 2 *B*), and were either not treated with H_2O_2 or incubated with 10 mM of H_2O_2. We found that 10 mM of H_2O_2 induced an initial Ca^{2+} increase in both control transfected cells and cells transfected with STIM1/Orai1 siRNA (Fig. 2 *B*). The initial Ca^{2+} increase was analyzed as the average intracellular Ca^{2+} concentration at 1180 s (before application of Tg) and plotted for each condition (Fig. 2 *C*). Upon incubation with 10 mM of H_2O_2, the initial Ca^{2+} increase remained unchanged after knockdown of STIM1 and Orai1 (Fig. 2 *C*). Therefore, we conclude that the initial Ca^{2+} increase is independent of STIM1/Orai1-mediated signaling.

In addition, this experiment demonstrates that the initial Ca^{2+} increase is not based on Ca^{2+} release from intracellular Ca^{2+} stores. Ca^{2+} release from intracellular Ca^{2+} stores leads to an activation of SOCE. Therefore, STIM1 and Orai1 knockdown would result in a reduction of the initial Ca^{2+} increase, which we did not observe.

To analyze the Tg-induced Ca^{2+} increase for each cell, we subtracted the Ca^{2+} level before application of Tg

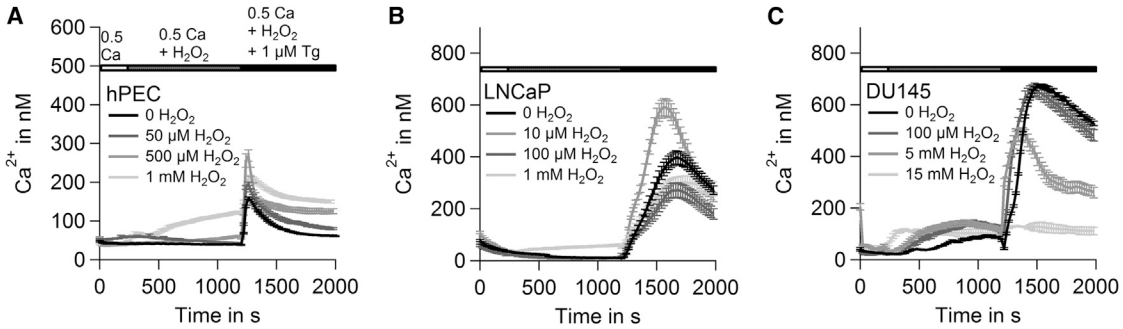

FIGURE 1 ROS dependence of Ca^{2+} signaling in hPECs, LNCaP, and DU145. (*A*) Average $[Ca^{2+}]_i$ responses (mean ± SE) from a Fura-2-based Ca^{2+} imaging assay when hPECs were incubated with different concentrations of H_2O_2 and 1 μM Tg was added ($n = 93$ for 0 H_2O_2, $n = 146$ for 50 μM H_2O_2, $n = 67$ for 500 μM H_2O_2, and $n = 180$ for 1 mM H_2O_2). (*B*) Same as (*A*) for LNCaP cells ($n = 144$ for 0 μM H_2O_2, $n = 69$ for 10 μM H_2O_2, $n = 70$ for 100 μM H_2O_2, and $n = 46$ for 1 mM H_2O_2). (*C*) Same as (*A*) and (*B*) for DU145 ($n = 172$ for 0 μM H_2O_2, $n = 43$ for 100 μM H_2O_2, $n = 57$ for 5 mM H_2O_2, and $n = 55$ for 15 mM H_2O_2).

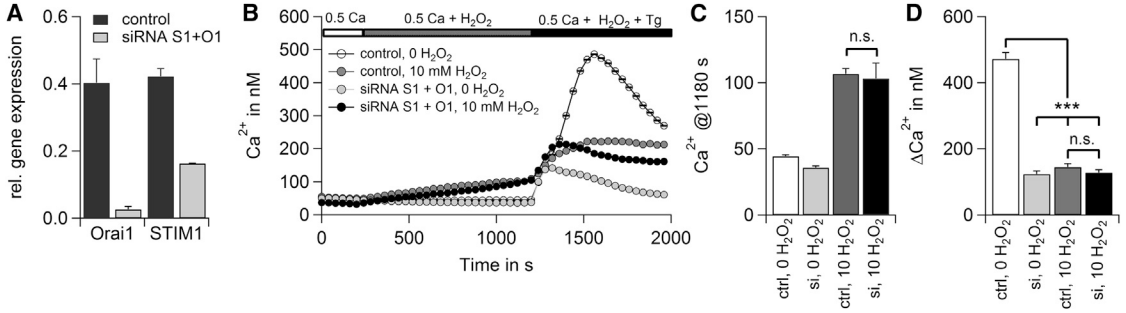

FIGURE 2 Dependence of the initial Ca^{2+} increase and Tg-induced intracellular Ca^{2+} increase on the STIM1/Orai1 machinery in LNCaP cells. (*A*) qRT-PCR analysis of Orai1 and STIM1 expression levels in LNCaP cells transfected with control RNA or siRNA targeting STIM1 and Orai1 normalized to TBP. (*B*) Average $[Ca^{2+}]_i$ responses (mean ± SE) from a Fura-2-based Ca^{2+} imaging assay when cells from (*A*) were not treated with H_2O_2 or were incubated with 10 mM of H_2O_2 and 1 μM of Tg was added ($n = 135$ for control RNA, 0 H_2O_2; $n = 98$ for control RNA and 10 mM H_2O_2; $n = 74$ for siRNA STIM1 and Orai1 and 0 H_2O_2; $n = 49$ for siRNA STIM1 and Orai1 and 10 mM H_2O_2). (*C*) Average $[Ca^{2+}]_i$ responses (mean ± SE) from cells in (*B*) at $t = 1180$ s. (*D*) For each cell, the Ca^{2+} before application of Tg was subtracted from the maximal Ca^{2+} after application of Tg. The average ΔCa^{2+} values for cells in (*B*) are plotted.

from the maximal Ca^{2+} level after application of Tg. The average ΔCa^{2+} is plotted for each condition in Fig. 2 *D*. When STIM1 and Orai1 were knocked down or cells were incubated with 10 mM of H_2O_2, or both, ΔCa^{2+} was significantly reduced to the same level (Fig. 2 *D*). When cells were incubated with 10 mM of H_2O_2, knockdown of STIM1 and Orai1 did not significantly reduce the remaining Ca^{2+} elevation. Consequently, this remaining Ca^{2+} elevation is independent of the STIM1/Orai1 machinery and for the most part is based on Tg-induced Ca^{2+} release from intracellular Ca^{2+} stores, as shown in a previous study (34). As the remaining Ca^{2+} elevation was the same in all three conditions (when STIM1 and Orai1 were knocked down or cells were incubated with 10 mM of H_2O_2, or both), we conclude that our further analysis of the H_2O_2-induced block of SOCE may include a small offset, but half minimal inhibitory concentrations were not affected. We performed the same set of experiments in DU145 and obtained very similar results (Fig. S1 *A* in the Supporting Material). Taken together, these results suggest that the initial effect is independent of Ca^{2+} release from intracellular stores and SOCE. Next, to investigate the H_2O_2-induced block of SOCE, we analyzed ΔCa^{2+}.

hPECs and prostate cancer cells differ in the initial increase of Ca^{2+} upon incubation with H_2O_2

Upon incubation with H_2O_2, the initial increase of Ca^{2+} varied among the tested cells. Incubation of hPECs with H_2O_2 concentrations of ≥ 100 μM induced an initial increase of intracellular Ca^{2+} levels, up to ~150 nM when cells were incubated with 1 mM of H_2O_2 (Fig. 3 *A*). In LNCaP and DU145, incubation with H_2O_2 induced an initial increase of intracellular Ca^{2+} (Fig. 3 *B*), and we detected maximal intracellular Ca^{2+} upon incubation with 300 μM and 1 mM of H_2O_2, respectively. Incubation of LNCaP and DU145 with H_2O_2 concentrations exceeding these maxima blocked the initial Ca^{2+} increase.

hPECs and prostate cancer cells differ in ΔCa^{2+} upon incubation with H_2O_2

Addition of the SERCA inhibitor Tg depleted intracellular Ca^{2+} stores and activated SOCE. The H_2O_2 dose dependency of ΔCa^{2+} in hPECs, LNaP, and DU145 is shown in Fig. 4, *A* and *B*.

In hPECs, ΔCa^{2+} was increased by incubation with H_2O_2 up to a concentration of 500 μM. When cells were incubated with 1 mM H_2O_2, the increment was reduced but ΔCa^{2+} was still elevated compared with ΔCa^{2+} at low H_2O_2 concentrations (Fig. 4 *A*). Upon incubation with H_2O_2 concentrations above 1 mM, hPECs started to detach during the measurements; however, from our data, we conclude that the IC_{50} of the H_2O_2-induced block of ΔCa^{2+} is above 1 mM.

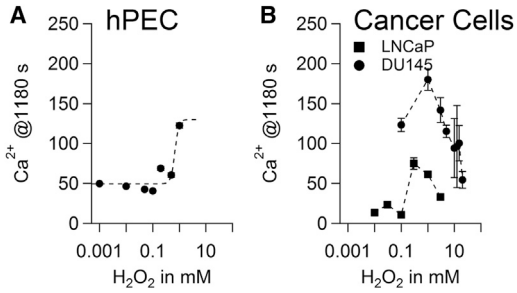

FIGURE 3 Initial H_2O_2-induced Ca^{2+} increase in hPEC and cancer cell lines. (*A*) Initial increase of intracellular Ca^{2+} when hPECs were incubated for 1000 s with H_2O_2 (before Tg was added). Same cells as in Fig. 1 *A*; $n = 71$ for 10 nM H_2O_2, $n = 46$ for 100 nM H_2O_2, $n = 133$ for 1 μM H_2O_2, $n = 158$ for 10 μM H_2O_2, $n = 160$ for 100 μM H_2O_2, and $n = 157$ for 300 μM H_2O_2. (*B*) Initial increase of Ca^{2+} when LNCaP or DU145 was incubated for 1000 s with H_2O_2 (before Tg was added). For LNCaP, same cells as in Fig. 1 *B*; $n = 67$ for 30 μM H_2O_2, and $n = 61$ for 3 mM H_2O_2. For DU145, same cells as in Fig. 1 *C*; $n = 29$ for 1 mM H_2O_2, $n = 32$ for 3 mM H_2O_2, $n = 64$ for 10 mM H_2O_2, $n = 84$ for 12.5 mM H_2O_2, and $n = 45$ for 20 mM H_2O_2.

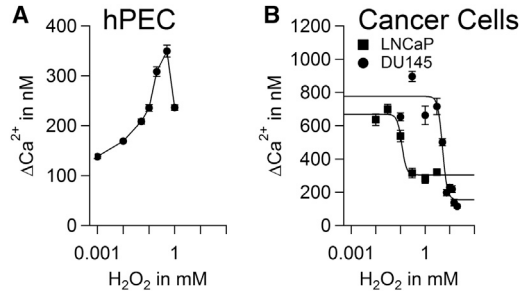

FIGURE 4 ΔCa^{2+} in hPEC and cancer cell lines. (*A*) ΔCa^{2+} after addition of Tg in hPECs upon incubation with different H_2O_2 concentrations, showing the same cells as in Figs. 1 *A* and 3 *A*. The line was drawn to guide the eye. (*B*) ΔCa^{2+} in LNCaP and DU145 cells after addition of Tg upon incubation with different H_2O_2 concentrations. Average ΔCa^{2+} values (mean ± SE) are plotted versus H_2O_2 concentration; same cells as in Figs. 1, *B* and *C*, and 3 *B*; $n = 44$ for 7.5 mM H_2O_2 for DU145. Data were fitted with a Hill function (please see text and Table 1 for IC_{50} values).

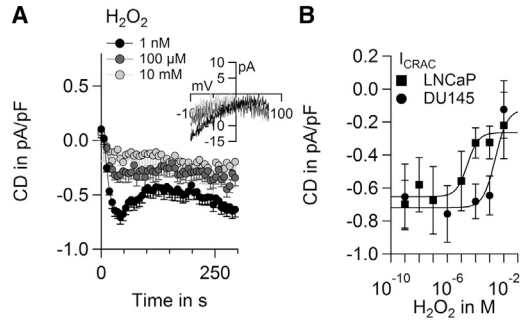

FIGURE 5 Inhibition of I_{CRAC} by H_2O_2 in cancer cell lines. (*A*) I_{CRAC} in LNCaP cells incubated with different concentrations of H_2O_2 (*black curve*, $n = 14$, 1 nM H_2O_2; *dark gray curve*, $n = 8$, 100 μM H_2O_2; *light gray curve*, $n = 9$, 10 mM H_2O_2) and corresponding I/V (*inset*). (*B*) Dose responses for H_2O_2-induced block of I_{CRAC} in LNCaP (same cells as in *A*; $n = 15$ for 10 nM H_2O_2, $n = 14$ for 100 nM H_2O_2, $n = 12$ for 1 μM H_2O_2, $n = 15$ for 10 μM H_2O_2, and $n = 9$ for 1 mM H_2O_2) and DU145 ($n = 10$ for 1 nM H_2O_2, $n = 8$ for 100 nM H_2O_2, $n = 5$ for 1 μM H_2O_2, $n = 8$ for 10 μM H_2O_2, $n = 5$ for 1 mM H_2O_2, and $n = 4$ for 10 mM H_2O_2).

Upon addition of Tg, the maximal increase in ΔCa^{2+} was detected with 30 μM and 300 μM of H_2O_2 in LNCaP and DU145, respectively. The dose-response curves for the H_2O_2-induced inhibition of ΔCa^{2+} in LNCaP and DU145 are shown in Fig. 4 *B*. The data were fitted with a Hill equation, and the IC_{50} values for H_2O_2-induced inhibition of ΔCa^{2+} were 114 μM and 5.1 mM for LNCaP and DU145 cells, respectively.

Upon incubation with H_2O_2, LNCaP and DU145 differ in I_{CRAC}

As ΔCa^{2+} includes a small offset that is mainly caused by Ca^{2+} release from intracellular stores, we challenged our concept and directly assessed the H_2O_2-induced block of CRAC channels. For this purpose, we incubated LNCaP and DU145 cells with various concentrations of H_2O_2 and performed a whole-cell patch-clamp analysis. Under these conditions, we detected Ca^{2+} currents via I_{CRAC} channels without any contribution of Ca^{2+} from intracellular stores.

I_{CRAC} was evoked with 50 μM of IP_3 and 10 mM of BAPTA in the patch pipette. For LNCaP, the CD was plotted versus time (Fig. 5 *A*; corresponding current-voltage curves are shown in Fig. 5 *A*, *inset*).

With increasing H_2O_2 concentrations, CD development in LNCaP and DU145 cells was blocked in a dose-dependent manner (Fig. 5 *B*). For the H_2O_2-induced block of I_{CRAC}, the dose-response curves exhibit an IC_{50} of 26.6 μM for LNCaP cells and 2.5 mM for DU145 cells (Fig. 5 *B*). This analysis shows that a higher ratio of Orai3/Orai1 is accompanied by a higher IC_{50} for the H_2O_2-induced block of I_{CRAC}. In our hands, a gigaseal could not be formed with hPECs upon incubation with H_2O_2; therefore, under these conditions, I_{CRAC} could not be detected via the patch-clamp technique in these cells.

hPECs, LNCaP, DU145, and PC3 differ in cell viability upon incubation with H_2O_2

To compare the viability of hPECs and prostate cancer cell lines upon incubation with H_2O_2, we performed fluorescence-based viability assays. The H_2O_2-induced decrease of cell viability exhibited an IC_{50} of ~6 mM in hPECs, ~2 mM in PC3, 871 μM in DU145, and 422 μM in LNCaP (Fig. 6). These findings clearly support the concept of higher ROS sensitivity in prostate cancer lines than in hPECs.

Analysis of Orai3/Orai1 ratios and the H_2O_2-dependent block of SOCE and cell viability

We next combined our data and previous findings (34,35) regarding Orai1/Orai3 mRNA ratios and the dependence of SOCE and cell viability on H_2O_2 in different cell types (summarized in Table 1).

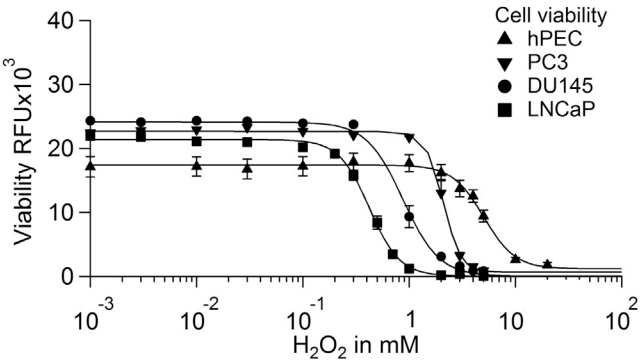

FIGURE 6 Fluorescence-based viability assay of hPECs and cancer cell lines upon incubation with different concentrations of H_2O_2. Fluorescence intensity is plotted versus H_2O_2 concentration for LNCaP (■), DU145 (●), PC3 (▼), and hPEC (▲). The sample size was $n = 12$ for LNCaP, $n = 9$ for DU145, $n = 3$ for PC3, and $n = 22$ from three donors for hPEC.

TABLE 1 Orai1/Orai3 Ratio, SOCE, and cell viability

Cell Type	Orai1/Orai3	IC_{50} H_2O_2-Induced Block of SOCE (μM)	IC_{50} H_2O_2-Induced Block of I_{CRAC} (μM)	IC_{50} H_2O_2-Dependent Viability (μM)
Naive T_H cell	70 (35)	7 (35)	ND	39 (35)
Effector T_H cell	25 (35)	51 (35)	ND	199 (35)
LNCaP	26 (34)	114	26	422
DU145	17 (34)	5114	2500	871
PC3	8	ND	ND	2085
Primary prostate epithelial cells	4 (34)	>1000	ND	5947

The table lists the Orai1/Orai3 ratios of the indicated cell types and IC_{50} values for the H_2O_2-induced block of SOCE, H_2O_2-induced block of I_{CRAC}, and H_2O_2-dependent cell viability.

We analyzed the correlation between the H_2O_2-dependent block of SOCE (ΔCa^{2+}) and dependence of viability on the Orai1/Orai3 ratio. For this purpose, we decided to use the inverse Orai1/Orai3 ratio and instead plot Orai3/Orai1. For prostate-derived cells, a detailed representation of Orai1 and Orai3 mRNA levels and the corresponding Orai3/Orai1 ratios is given in Fig. S2.

In Fig. 7 *A*, the logarithmic IC_{50} of the H_2O_2-induced block of SOCE is plotted against different Orai3/Orai1 ratios expressed by several types of cells. When we analyze the correlation between the Orai3/Orai1 ratio and the logarithmic IC_{50} for the H_2O_2-induced block of SOCE, we find a Pearson's coefficient of 0.97, reflecting the very strong correlation between the two parameters. Fig. 7 *B* demonstrates the relationship between Orai3/Orai1 ratios and cell viability. Here, we included data from PC3 cells without analyzing Ca^{2+} signaling in these cells in depth. With our protocol, we cannot determine IC_{50} for the H_2O_2-induced block of SOCE because in PC3 the initial effect depends on STIM1/Orai1, whereas the Tg-induced Ca^{2+} is nearly independent of STIM1/Orai1 (Fig. S3). The Pearson's coefficient between the Orai3/Orai1 ratio and cell viability is 0.99, reflecting the very strong correlation between the Orai3/Orai1 ratio and H_2O_2-induced inhibition of cell viability. When the IC_{50} of the H_2O_2-induced block of cell viability is plotted against the H_2O_2-induced block of SOCE, the dependency can best be described with a Hill function (Fig. 7 *C*). The Pearson's coefficient for the logarithmic data is 0.91, reflecting the strong correlation between the H_2O_2-induced block of SOCE and cell viability.

Effect of a siRNA-based knockdown of Orai3 on Ca^{2+} signaling and cell viability

To directly determine the role of Orai3 in the H_2O_2-induced block of SOCE and cell viability, we performed a siRNA-based knockdown of Orai3. Upon knockdown, Orai3 mRNA was reduced (Fig. 8 *A*). Upon knockdown of Orai3, no specific effect on the IC_{50} of H_2O_2-induced inhibition of ΔCa^{2+} (Fig. 8 *B*) and cell viability (Fig. 8 *C*) could be detected. The cell transfection led to a general shift in the IC_{50} for the H_2O_2-induced inhibition of ΔCa^{2+} and cell viability.

DISCUSSION

Our data on H_2O_2-dependent cell viability support the concept that hPECs are less sensitive to ROS than LNCaP and DU145. This finding is in line with an earlier study

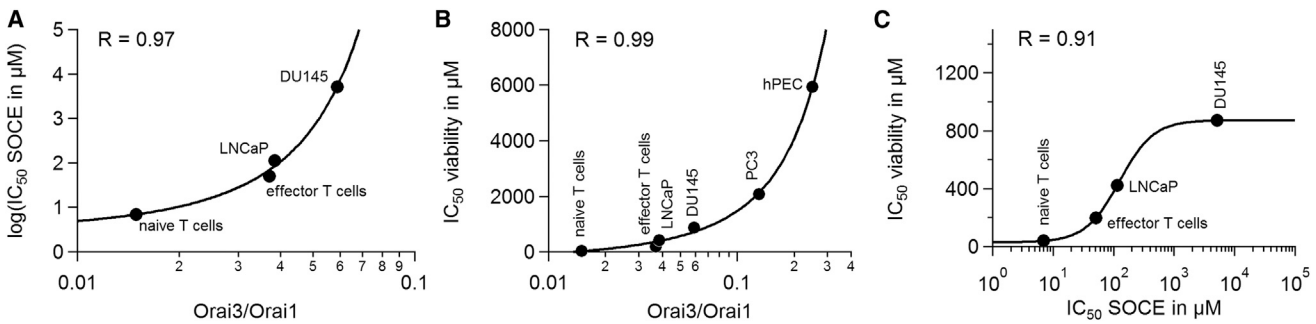

FIGURE 7 Correlation between the Orai3/Orai1 ratio and the H_2O_2-dependent block of SOCE and cell viability. (*A*) The logarithmic IC_{50} of the H_2O_2-induced block of SOCE is plotted against the Orai3/Orai1 ratio in different cell types (naive T cells (35), effector T cells (35), LNCaP cells (34), and DU145 cells (34)). Data were fitted with an exponential fit function and Pearson's coefficient is indicated as the R value. (*B*) The IC_{50} of the H_2O_2-induced block of viability is plotted against the Orai3/Orai1 ratio of the same cell types as in (*A*), as well as in PC3 and hPEC. Data were fitted with a stretched exponential fit function and Pearson's coefficient is indicated as the R value. (*C*) The IC_{50} of the H_2O_2-induced block of viability is plotted versus the IC_{50} of the H_2O_2-induced block of SOCE. Data were fitted with a Hill function and Pearson's coefficient is indicated as the R value.

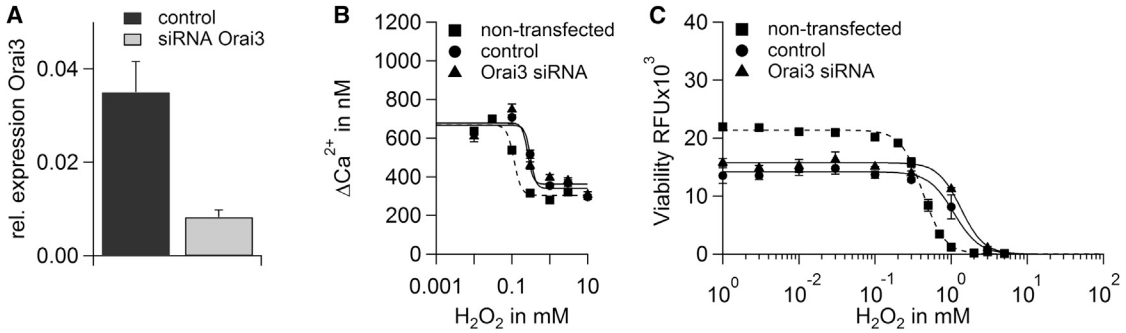

FIGURE 8 Effect of a siRNA-based knockdown of Orai3 on Ca^{2+} signaling and cell viability. (*A*) qRT-PCR analysis of Orai3 expression levels in LNCaP cells transfected with control RNA or siRNA targeting Orai3 normalized to TBP. (*B*) Average ΔCa^{2+} from a Fura-2-based Ca^{2+} imaging assay when cells were nontransfected (same data as in Fig. 4 *B*), control transfected ($n = 76$ for 0.01 mM H_2O_2, $n = 144$ for 0.1 mM H_2O_2, $n = 164$ for 0.3 mM H_2O_2, $n = 159$ for 1 mM H_2O_2, $n = 157$ for 3 mM H_2O_2 and $n = 82$ for 10 mM H_2O_2), or transfected with siRNA targeting Orai3 ($n = 84$ for 0.01 mM H_2O_2, $n = 146$ for 0.1 mM H_2O_2, $n = 165$ for 0.3 mM H_2O_2, $n = 182$ for 1 mM H_2O_2, $n = 152$ for 3 mM H_2O_2, and $n = 94$ for 10 mM H_2O_2). (*C*) Viability assay of cells in (*B*) ($n = 2$); for nontransfected cells, the same data as in Fig. 6 were used.

that demonstrated that cells derived from prostate cancer tumors are more sensitive to arsenic-trioxide-induced ROS compared with normal prostate epithelium cells (49). It was shown that blocking the ROS-scavenging system of prostate cancer cells shifted the IC_{50} for arsenic-trioxid-induced cell death in prostate cancer cells to clinical achievable concentrations, with a negligible cytotoxicity for normal cells. It is known that in prostate cancer cells, ROS induce elevations of intracellular Ca^{2+} (12,13). Here, we investigated the H_2O_2-induced initial rise of intracellular Ca^{2+}, the H_2O_2-induced amplification of ΔCa^{2+}, the block of SOCE, and cell viability upon incubation with ROS in hPECs and prostate cancer cell lines. The ROS-induced initial increase of Ca^{2+} is independent of the STIM1/Orai1 machinery and may be caused by Ca^{2+} channels, e.g., TRP channels that are activated or modulated by ROS, including TRPM2, TRPC5, TRPV1, and TRPA1 (14,16). The initial H_2O_2-induced increase of intracellular Ca^{2+} is maximally activated at lower concentrations of H_2O_2 in LNCaP cells than in hPECs and DU145 (300 μM vs. 1 mM H_2O_2). In prostate cancer cell lines, these values reflect the maxima, and the initial Ca^{2+} increase is blocked upon incubation with higher concentrations of H_2O_2. In hPECs, 1 mM of H_2O_2 induces the maximal initial increase of intracellular Ca^{2+}. The detection of Ca^{2+} signals from cells incubated with higher concentrations of H_2O_2 was technically not feasible. It is known that ROS-induced transcription factors that activate ROS-scavenging systems (e.g., NF-E2-related factor 2) (50) depend on elevation of intracellular Ca^{2+} (51). Hence, the block of initial ROS-induced Ca^{2+} signaling in cancer cell lines may contribute to their higher sensitivity to ROS.

SOCE is activated during proliferation; however, elevated SOCE signals can drive cells into apoptosis (52). When cells were preincubated with different H_2O_2 concentrations, the maximal amplification of ΔCa^{2+} occurred with 500 μM of H_2O_2 in hPECs, 30 μM of H_2O_2 in LNCaP, and 300 μM of H_2O_2 in DU145. Thus, in cancer cell lines, these maximally amplified ΔCa^{2+} signals at lower H_2O_2 concentrations may contribute to the overall higher sensitivity of cell viability to ROS.

Within the last few years, several reports have demonstrated a role for Orai3 in breast cancer (53–56). Two very recent studies reported controversial results regarding the role of Orai3 in prostate cancer. Dubois et al. (57) found elevated Orai3 expression levels in prostate cancer tissue samples. In their study, elevated levels of Orai3 led to increased formation of arachidonic-acid-induced Ca^{2+} channels by Orai1/Orai3 heteromers and a lower number of homomeric Orai1 SOCE channels. Thus, the elevated Orai3 levels may act as a switch and lead to increased arachidonic-acid-induced proliferation and decreased Orai1-dependent apoptosis (57,58). In contrast to Dubois et al. (57), we found a downregulation of Orai3 in prostate cancer tissue samples, an outstandingly low Orai1/Orai3 ratio of ~4 in hPECs, and elevated Orai1/Orai3 ratios in prostate cancer cell lines, with consequences for SOCE signaling in the membrane androgen receptor pathway and the pharmacological profile of I_{CRAC} (34). The H_2O_2-dependent block of SOCE (ΔCa^{2+}) differs among hPECs ($IC_{50} > 1$ mM), DU145 (IC_{50} ~5 mM), and LNCaP (IC_{50} ~114 μM). In combination with previous findings (34,35), our results demonstrate a strong correlation between the Orai3/Orai1 ratio and the ROS sensitivity of SOCE and cell viability. Taken together, these findings support the concept of heteromeric store-operated Orai1/Orai3 channels. However, upon cell transfection, the IC_{50} values of the H_2O_2-induced block of SOCE and cell viability exhibited unspecific shifts, as described previously (35). This unspecific shift may cover specific effects of Orai3 knockdown and thus prevent the acquisition of direct evidence. The correlation between the ROS-dependent block of SOCE and cell viability demonstrates that cells need functional SOCE Ca^{2+} signaling for survival and that the ROS-induced block of SOCE

contributes to decreased cell viability when ROS are increased. The apparent IC_{50} of the H_2O_2-induced block of SOCE in DU145 (~5 mM) and hPECs (>1 mM) points to a blocking mechanism that could be independent of Orai3/Orai1 ratios. In these cells, all I_{CRAC} channels may be Orai3/Orai1 heteromeric channels, and one Orai3 subunit is sufficient to abolish the ROS sensitivity of SOCE (37). An alternative explanation is that increasing H_2O_2 levels lead to intracellular acidification (59) and CRAC channels are inhibited by intracellular acidification (60). It has been suggested that STIM1/Orai1 uncouple at low intracellular pH and Ca^{2+} influx via Orai channels is abolished (61). To test this hypothesis, we performed patch-clamp experiments to determine whether the H_2O_2-induced block was still apparent when we used pH 8 in the patch pipette (Fig. S4). Indeed, the block was not abolished, pointing to a channel-specific mechanism rather than an unspecific block. On the other hand, it was previously demonstrated in snail neurons that even under buffering conditions, pH microdomains below the plasma membrane could be formed (62). Thus, we cannot exclude the possibility of a channel-unspecific mechanism such as acidic pH, decoupling of STIM/Orai complexes, induction of high Ca^{2+} levels, and/or membrane depolarization.

In the future, therapeutic strategies based on ROS induction may include the appropriate concentrations of drugs targeting SOCE channels to reduce the viability of prostate cancer cells without affecting nontransformed cells, as there is a clear role for Ca^{2+} in ROS-mediated signaling in prostate cancer. Finally, the overall high Orai3/Orai1 ratios in hPEC and androgen-insensitive cancer cells contribute to their ROS resistance and thereby may have a share in making the prostate one of the most prominent cancer susceptible organs.

CONCLUSIONS

In this study, we investigated H_2O_2-dependent Ca^{2+} signaling in hPECs from healthy tissue and prostate cancer cell lines (LNCaP, DU145, and PC3). ROS-induced changes in Ca^{2+} signaling reflect the contributions of very different enzymes, including Ca^{2+} transporters and ROS-producing and -scavenging enzymes. Our findings suggest that the block of ROS-induced initial Ca^{2+} elevations in prostate cancer cells, as well as the amplification of ΔCa^{2+} and the H_2O_2-dependent block of SOCE at lower concentrations of H_2O_2, could contribute to the higher sensitivity of prostate cancer cells to ROS-induced cell death. In addition, our findings regarding the H_2O_2-dependent block of SOCE in hPECs and cancer cell lines support our concept of heteromeric store-operated Orai1/Orai3 channels in hPECs and store-operated Orai channels characterized by elevated Orai1/Orai3 ratios in prostate cancer cells.

SUPPORTING MATERIAL

Four figures are available at http://www.biophysj.org/biophysj/supplemental/S0006-3495(15)00816-4.

AUTHOR CONTRIBUTIONS

C.P. designed the study, analyzed data, and wrote the manuscript. C.H., T.K., S.K., and K.D. performed experiments, analyzed data, helped design the study, and helped write the manuscript. I.B. helped design the study and develop the manuscript. V.J. and M.S. helped design the study.

ACKNOWLEDGMENTS

We thank Helga Angeli, Andrea Armbrüster, Petra Frieß, Sandra Janku, Gertrud Schwär, and Cora Stephan for technical support, and Sandra Janku for a careful reading of the manuscript. C.P. thanks Markus Hoth for constant and extraordinary support.

This study was supported by grants from the Deutsche Forschungsgemeinschaft (SFB 1027 (C4) and BO 3643/3-1 to I.B., and SFB 894 (A2) and PE1478/5-1 to C.P.). I.B. received funding from the HOMFORexcellent program of Saarland University. V.J. received funding from the Stiftung Europrofession and HOMFOR of Saarland University.

REFERENCES

1. Malins, D. C., P. M. Johnson, …, M. A. Vinson. 2001. Age-related radical-induced DNA damage is linked to prostate cancer. *Cancer Res.* 61:6025–6028.
2. Miyake, H., I. Hara, …, H. Eto. 2004. Oxidative DNA damage in patients with prostate cancer and its response to treatment. *J. Urol.* 171:1533–1536.
3. Bostwick, D. G., E. E. Alexander, …, T. D. Oberley. 2000. Antioxidant enzyme expression and reactive oxygen species damage in prostatic intraepithelial neoplasia and cancer. *Cancer.* 89:123–134.
4. Khandrika, L., B. Kumar, …, H. K. Koul. 2009. Oxidative stress in prostate cancer. *Cancer Lett.* 282:125–136.
5. Lim, S. D., C. Sun, …, R. S. Arnold. 2005. Increased Nox1 and hydrogen peroxide in prostate cancer. *Prostate.* 62:200–207.
6. Harrison, I. P., and S. Selemidis. 2014. Understanding the biology of reactive oxygen species and their link to cancer: NADPH oxidases as novel pharmacological targets. *Clin. Exp. Pharmacol. Physiol.* 41:533–542.
7. Yang, Y., S. Karakhanova, …, A. V. Bazhin. 2013. Reactive oxygen species in cancer biology and anticancer therapy. *Curr. Med. Chem.* 20:3677–3692.
8. Paschos, A., R. Pandya, …, J. H. Pinthus. 2013. Oxidative stress in prostate cancer: changing research concepts towards a novel paradigm for prevention and therapeutics. *Prostate Cancer Prostatic Dis.* 16:217–225.
9. Rosado, J. A., P. C. Redondo, …, J. A. Pariente. 2006. Calcium signalling and reactive oxygen species in non-excitable cells. *Mini Rev. Med. Chem.* 6:409–415.
10. Yan, Y., C. L. Wei, …, J. Liu. 2006. Cross-talk between calcium and reactive oxygen species signaling. *Acta Pharmacol. Sin.* 27:821–826.
11. Gordeeva, A. V., R. A. Zvyagilskaya, and Y. A. Labas. 2003. Cross-talk between reactive oxygen species and calcium in living cells. *Biochemistry (Mosc.).* 68:1077–1080.
12. Kim, K. Y., H. J. Cho, …, S. C. Ahn. 2013. Interplay of reactive oxygen species, intracellular Ca2+ and mitochondrial homeostasis in the apoptosis of prostate cancer cells by deoxypodophyllotoxin. *J. Cell. Biochem.* 114:1124–1134.

13. Savino, 3rd, J. A., J. F. Evans, …, T. H. Carter. 2006. Multiple, disparate roles for calcium signaling in apoptosis of human prostate and cervical cancer cells exposed to diindolylmethane. *Mol. Cancer Ther.* 5:556–563.
14. Bogeski, I., R. Kappl, …, B. A. Niemeyer. 2011. Redox regulation of calcium ion channels: chemical and physiological aspects. *Cell Calcium.* 50:407–423.
15. Grupe, M., G. Myers, …, A. Fleig. 2010. Activation of store-operated I(CRAC) by hydrogen peroxide. *Cell Calcium.* 48:1–9.
16. Shimizu, S., N. Takahashi, and Y. Mori. 2014. TRPs as chemosensors (ROS, RNS, RCS, gasotransmitters). *Handbook Exp. Pharmacol.* 223:767–794.
17. Parekh, A. B., and R. Penner. 1995. Activation of store-operated calcium influx at resting InsP3 levels by sensitization of the InsP3 receptor in rat basophilic leukaemia cells. *J. Physiol.* 489:377–382.
18. Bogeski, I., T. Kilch, and B. A. Niemeyer. 2012. ROS and SOCE: recent advances and controversies in the regulation of STIM and Orai. *J. Physiol.* 590:4193–4200.
19. Lewis, R. S. 2011. Store-operated calcium channels: new perspectives on mechanism and function. *Cold Spring Harb. Perspect. Biol.* 3: a003970.
20. Ji, W., P. Xu, …, L. Chen. 2008. Functional stoichiometry of the unitary calcium-release-activated calcium channel. *Proc. Natl. Acad. Sci. USA.* 105:13668–13673.
21. Penna, A., A. Demuro, …, M. D. Cahalan. 2008. The CRAC channel consists of a tetramer formed by Stim-induced dimerization of Orai dimers. *Nature.* 456:116–120.
22. Demuro, A., A. Penna, …, I. Parker. 2011. Subunit stoichiometry of human Orai1 and Orai3 channels in closed and open states. *Proc. Natl. Acad. Sci. USA.* 108:17832–17837.
23. Madl, J., J. Weghuber, …, G. J. Schütz. 2010. Resting state Orai1 diffuses as homotetramer in the plasma membrane of live mammalian cells. *J. Biol. Chem.* 285:41135–41142.
24. Maruyama, Y., T. Ogura, …, C. Sato. 2009. Tetrameric Orai1 is a teardrop-shaped molecule with a long, tapered cytoplasmic domain. *J. Biol. Chem.* 284:13676–13685.
25. Thompson, J. L., and T. J. Shuttleworth. 2013. How many Orai's does it take to make a CRAC channel? *Sci. Rep.* 3:1961.
26. Hou, X., L. Pedi, …, S. B. Long. 2012. Crystal structure of the calcium release-activated calcium channel Orai. *Science.* 338:1308–1313.
27. Wu, M. M., E. D. Covington, and R. S. Lewis. 2014. Single-molecule analysis of diffusion and trapping of STIM1 and Orai1 at endoplasmic reticulum-plasma membrane junctions. *Mol. Biol. Cell.* 25:3672–3685.
28. Balasuriya, D., S. Srivats, …, J. M. Edwardson. 2014. Atomic force microscopy (AFM) imaging suggests that stromal interaction molecule 1 (STIM1) binds to Orai1 with sixfold symmetry. *FEBS Lett.* 588:2874–2880.
29. Amcheslavsky, A., M. L. Wood, …, M. D. Cahalan. 2015. Molecular biophysics of Orai store-operated Ca2+ channels. *Biophys. J.* 108: 237–246.
30. Zhang, S. L., J. A. Kozak, …, M. D. Cahalan. 2008. Store-dependent and -independent modes regulating Ca2+ release-activated Ca2+ channel activity of human Orai1 and Orai3. *J. Biol. Chem.* 283: 17662–17671.
31. Lis, A., C. Peinelt, …, R. Penner. 2007. CRACM1, CRACM2, and CRACM3 are store-operated Ca2+ channels with distinct functional properties. *Curr. Biol.* 17:794–800.
32. Gwack, Y., S. Srikanth, …, A. Rao. 2007. Biochemical and functional characterization of Orai proteins. *J. Biol. Chem.* 282:16232–16243.
33. Schindl, R., I. Frischauf, …, C. Romanin. 2009. Plasticity in Ca2+ selectivity of Orai1/Orai3 heteromeric channel. *Proc. Natl. Acad. Sci. USA.* 106:19623–19628.
34. Holzmann, C., T. Kilch, …, C. Peinelt. 2013. ICRAC controls the rapid androgen response in human primary prostate epithelial cells and is altered in prostate cancer. *Oncotarget.* 4:2096–2107.
35. Bogeski, I., C. Kummerow, …, B. A. Niemeyer. 2010. Differential redox regulation of ORAI ion channels: a mechanism to tune cellular calcium signaling. *Sci. Signal.* 3:ra24.
36. Mignen, O., J. L. Thompson, and T. J. Shuttleworth. 2009. The molecular architecture of the arachidonate-regulated Ca2+-selective ARC channel is a pentameric assembly of Orai1 and Orai3 subunits. *J. Physiol.* 587:4181–4197.
37. Alansary, D., I. Bogeski, and B. A. Niemeyer. 2015. Facilitation of Orai3 targeting and store-operated function by Orai1. *Biochim. Biophys. Acta.* 1853:1541–1550.
38. Gulaboski, R., I. Bogeski, …, R. Kappl. 2013. Hydroxylated derivatives of dimethoxy-1,4-benzoquinone as redox switchable earth-alkaline metal ligands and radical scavengers. *Sci. Rep.* 3:1865.
39. Bufe, B., T. Schumann, …, F. Zufall. 2015. Recognition of bacterial signal peptides by mammalian formyl peptide receptors: a new mechanism for sensing pathogens. *J. Biol. Chem.* 290:7369–7387.
40. Davidson, S. M., and M. R. Duchen. 2006. Calcium microdomains and oxidative stress. *Cell Calcium.* 40:561–574.
41. Singleton, P. A., S. Pendyala, …, V. Natarajan. 2009. Dynamin 2 and c-Abl are novel regulators of hyperoxia-mediated NADPH oxidase activation and reactive oxygen species production in caveolin-enriched microdomains of the endothelium. *J. Biol. Chem.* 284:34964–34975.
42. Kaludercic, N., S. Deshwal, and F. Di Lisa. 2014. Reactive oxygen species and redox compartmentalization. *Front. Physiol.* 5:285.
43. Gmyrek, G. A., M. Walburg, …, B. S. Knudsen. 2001. Normal and malignant prostate epithelial cells differ in their response to hepatocyte growth factor/scatter factor. *Am. J. Pathol.* 159:579–590.
44. Mantei, A., S. Rutz, …, A. Scheffold. 2008. siRNA stabilization prolongs gene knockdown in primary T lymphocytes. *Eur. J. Immunol.* 38:2616–2625.
45. Grynkiewicz, G., M. Poenie, and R. Y. Tsien. 1985. A new generation of Ca2+ indicators with greatly improved fluorescence properties. *J. Biol. Chem.* 260:3440–3450.
46. Alansary, D., T. Kilch, …, A. Lis. 2014. The minimal requirements to use calcium imaging to analyze ICRAC. *Cold Spring Harb. Protoc.* 2014:638–642.
47. Alansary, D., T. Kilch, …, A. Lis. 2014. Patch-clamp measurement of I_{CRAC} and ORAI channel activity. *Cold Spring Harb. Protoc.* 2014:602–607.
48. Alansary, D., T. Kilch, …, A. Lis. 2014. Measuring endogenous ICRAC and ORAI currents with the patch-clamp technique. *Cold Spring Harb. Protoc*. 2014:630–637.
49. Maeda, H., S. Hori, …, A. Kakizuka. 2004. Effective treatment of advanced solid tumors by the combination of arsenic trioxide and L-buthionine-sulfoximine. *Cell Death Differ.* 11:737–746.
50. Kobayashi, M., and M. Yamamoto. 2005. Molecular mechanisms activating the Nrf2-Keap1 pathway of antioxidant gene regulation. *Antioxid. Redox Signal.* 7:385–394.
51. Lee, J. M., A. Y. Shih, …, J. A. Johnson. 2003. NF-E2-related factor-2 mediates neuroprotection against mitochondrial complex I inhibitors and increased concentrations of intracellular calcium in primary cortical neurons. *J. Biol. Chem.* 278:37948–37956.
52. Roderick, H. L., and S. J. Cook. 2008. Ca2+ signalling checkpoints in cancer: remodelling Ca2+ for cancer cell proliferation and survival. *Nat. Rev. Cancer.* 8:361–375.
53. Faouzi, M., P. Kischel, …, H. Ouadid-Ahidouch. 2013. ORAI3 silencing alters cell proliferation and cell cycle progression via c-myc pathway in breast cancer cells. *Biochim. Biophys. Acta.* 1833: 752–760.
54. Motiani, R. K., I. F. Abdullaev, and M. Trebak. 2010. A novel native store-operated calcium channel encoded by Orai3: selective requirement of Orai3 versus Orai1 in estrogen receptor-positive versus estrogen receptor-negative breast cancer cells. *J. Biol. Chem.* 285: 19173–19183.

55. Motiani, R. K., X. Zhang, …, M. Trebak. 2013. Orai3 is an estrogen receptor α-regulated Ca^{2+} channel that promotes tumorigenesis. *FASEB J.* 27:63–75.

56. Faouzi, M., F. Hague, …, H. Ouadid-Ahidouch. 2011. Down-regulation of Orai3 arrests cell-cycle progression and induces apoptosis in breast cancer cells but not in normal breast epithelial cells. *J. Cell. Physiol.* 226:542–551.

57. Dubois, C., F. Vanden Abeele, …, N. Prevarskaya. 2014. Remodeling of channel-forming ORAI proteins determines an oncogenic switch in prostate cancer. *Cancer Cell.* 26:19–32.

58. Flourakis, M., V. Lehen'kyi, …, N. Prevarskaya. 2010. Orai1 contributes to the establishment of an apoptosis-resistant phenotype in prostate cancer cells. *Cell Death Dis.* 1:e75.

59. Ahmad, K. A., K. B. Iskandar, …, S. Pervaiz. 2004. Hydrogen peroxide-mediated cytosolic acidification is a signal for mitochondrial translocation of Bax during drug-induced apoptosis of tumor cells. *Cancer Res.* 64:7867–7878.

60. Beck, A., A. Fleig, …, C. Peinelt. 2014. Regulation of endogenous and heterologous Ca^{2+} release-activated Ca^{2+} currents by pH. *Cell Calcium.* 56:235–243.

61. Mancarella, S., Y. Wang, …, D. L. Gill. 2011. Hypoxia-induced acidosis uncouples the STIM-Orai calcium signaling complex. *J. Biol. Chem.* 286:44788–44798.

62. Schwiening, C. J., and D. Willoughby. 2002. Depolarization-induced pH microdomains and their relationship to calcium transients in isolated snail neurones. *J. Physiol.* 538:371–382.